CHEMISTRY JOURNAL OF MOLDOVA. General, Industrial and Ecological Chemistry. 2023, 18(1), 28-37
ISSN (p) 1857-1727 ISSN (e) 2345-1688
http://cjm.ichem.md
http://doi.org/10.19261/cjm.2023.1027

SYNTHESIS AND CHARACTERIZATION OF ZINC OXIDE AND CERIUM DIOXIDE NANOPARTICLES WITH POSSIBLE APPLICATION FOR NITRITE IONS REMOVAL IN WATERS

Zainab Abdul-Zahra and Rashed Rasheed *

Chemistry Branch, Applied Sciences Department, University of Technology, Al-Wehda nbhd., Baghdad 19006, Iraq
**e-mail: Rashed.T.Rasheed@uotechnology.edu.iq; phone: (+964) 07801670470*

Abstract. Nitrite ion, a characteristic pollutant, can be removed from water by reverse osmosis, distillation, or ion exchange resin. In this study, we removed it by using ZnO and CeO_2 nanoparticles. First, zinc hydroxide and cerium hydroxide were prepared by the hydrothermal method and heated at 90°C to dry. Second, they were annealed at 400°C to produce nanoparticles of ZnO and CeO_2, respectively. The obtained samples were characterized by X-ray diffraction to ascertain their structure and chemical composition. The surface morphology analysis of the nanoparticles was performed using scanning electron microscopy. Atomic force microscopy was employed to characterize the imaging surface and ascertain the surface roughness. The functional groups present at the surface of the nanoparticles were investigated using the Fourier transform infrared spectroscopy method. The optical properties of these particles were investigated using the UV-visible spectroscopy. Further, the produced nanoparticles were used to adsorb NO_2^- ions from aqueous solutions. The results showed that the nanoparticles which were heated at 90°C (hydroxide forms) presented a higher activity for nitrite ions removal than those that were heated at 400°C (oxide forms). This may be related to nitrite ions preferential adsorption to hydroxide forms rather than to oxide forms; in both cases (90°C and 400°C), zinc oxide nanoparticles presented higher nitrite removal activity.

Keywords: zinc oxide, cerium dioxide, nanoparticle, nitrite ion, pollutant, environment.

Received: 12 January 2023/ Revised final: 26 March 2023/ Accepted: 28 March 2023

Introduction

Nanoparticles are of incredible interest because of their extremely small size and large surface area to volume proportion, which lead to both physical and chemical differences in their properties [1]. Zinc oxide nanoparticles represent a white crystalline water insoluble powder [2], considered as one of the most promising inorganic oxides, with excellent magnetic, electrical, and optical properties. Zinc oxide nanoparticles are abundant in three forms: hexagonal wurtzite, rock salt, and cubic structures as semiconductors [3]. Different methods have been applied to synthesize zinc oxide nanoparticles such as the solution-gelatine (sol-gel) method [4], chemical vapor deposition, thermal decomposition, and alloy evaporation-deposition [5]. The temperature, solvents, and media of the experiment affect the particle morphology and particle size of synthesized zinc oxide nanoparticles.

Cerium dioxide nanoparticles (CNPs) have been widely utilized in various advanced technologies, such as solid oxide fuel cells, high-temperature oxidation protection materials, catalytic materials, oxygen sensors and solar cells, *etc.* [6]. CeO_2 nanoparticles have also been used as a free radical scavenger, to modulate oxidative stress in biological systems [7]. Various chemical methods have been reported on the synthesis of CeO_2 oxide nanoparticles such as reversed micelles route, co-precipitation, hydrothermal synthesis, forced hydrolysis, solvothermal synthesis, sol–gel process, pyrolysis, electrochemical methods, and sonochemical methods [8]. There are other methods used to prepare nanoparticles of zinc oxide and cerium dioxide [9], or cerium dioxide with other metals [10,11]. These methods used organic solvents in the preparation of these nanoparticles.

Nitrogenous pollutants such as nitrite and nitrate are bioaccumulated in water and soil, posing a threat to humans and plants [12]. A high concentration of nitrite in blood can cause the formation of methaemoglobin by reacting with haemoglobin Fe^{3+} ions, which causes a failure in oxygen-carrying ability [13]. There are many methods of decreasing nitrite ions, such as spectrophotometric chemiluminescent, electrochemical, chromatographic [14], reverse osmosis, ion exchange, electrodialysis, chemical

coagulation, membrane method, and adsorption, and each approach preents advantages and disadvantages [15]. Adsorption with nano-adsorbents is an appealing and promising approach for wastewater decontamination due to several advantages, including ease of use, cost effectiveness, environmental friendliness, and a high adsorption rate. The development of an effective adsorbent is the foundation of this technique's effectiveness [16]. Due to their unique physical, chemical, and surface qualities, adsorbent nanoparticles are often thought to be superior in removing nitrite [17].

This study aims to find an easy and inexpensive method to synthesize ZnO and CeO_2 nanoparticles by using urea as a precipitating agent, and using these nanoparticles as sorbents to remove contamination with nitrite ions in aqueous solutions.

Experimental Methods

Materials

Ammonium hydroxide, zinc acetate, and urea were purchased from Sigma-Aldrich. Cetrimethyl ammonium bromide (CTAB) and ceric sulphate tetrahydrate were obtained from Merck Company. Sodium nitrite, potassium iodide, and hydrochloric acid 37%) were obtained from British Drug Houses Company.

Synthesis of zinc oxide nanoparticles

Zinc oxide nanoparticles were synthesized by a hydrothermal technique (autoclave) according to a previously published method [18], by dissolving 3 g (16.36 mmol) of zinc acetate in distilled water (75 mL) and adding 0.981 g (16.35 mmol) of urea, and finally adding 1 g (2.74 mmol) of CTAB to this solution. Then the obtained solution was stirred with a magnetic stirrer at 25°C for 10 min, in a beaker until it became homogenous. Afterwards, the mixed solutions were placed in a Teflon-lined autoclave (100 mL), sealed, and kept at 200°C for 6 hours. The precipitate product (white colour) was washed several times with distilled water, then dried at 90°C for 1 hour and annealed at 400°C for 2 hours, according to Eqs.(1-4).

$$NH_2CONH_2 + 3H_2O \rightarrow 2NH_4OH + CO_2 \quad (1)$$

$$Zn(CH_3COO)_2 + 2\,NH_4OH \rightarrow Zn(OH)_2 + 2CH_3COONH_4 \quad (2)$$

$$NH_2CONH_2 + Zn(CH_3COO)_2 + 3\,H_2O \rightarrow Zn(OH)_2 + CO_2 + 2CH_3COONH_4 \quad (3)$$

$$Zn(OH)_2 \xrightarrow{\Delta} ZnO + H_2O \quad (4)$$

Synthesis of cerium dioxide nanoparticles

Cerium dioxide nanoparticles were prepared by a hydrothermal method using an autoclave according to a previously published method [8,19], by dissolving 3g (7.43 mmol) of cerium sulphate tetrahydrate in 75 mL of distilled water, then adding 1 g (16.66 mmol) of urea and finally dissolving 2 g (5.487 mmol) of CTAB in this solution. The mixture solution was stirred with a magnetic stirrer at 25°C (15 min) in a beaker until it became homogenous. Then it was put into a Teflon lined autoclave (100 mL), sealed and put into an oven at 200°C for 6 hours. After that, the precipitate was dried for 60 minutes at 90°C for 1 h, and at 400°C for 2 hours, according to the following Eqs.(5-7).

$$NH_2CONH_2 + 3H_2O \rightarrow 2NH_4OH + CO_2 \quad (5)$$

$$Ce(SO_4)_2.4H_2O + 4NH_4OH \rightarrow Ce(OH)_4 + 4H_2O + 2(NH_4)_2SO_4 \quad (6)$$

$$Ce(OH)_4 \xrightarrow{400℃} CeO_2 + 2H_2O \quad (7)$$

Instruments

The *UV-vis spectra* of nanoparticles' solutions ($1 \cdot 10^{-5}$ M, in ethanol solvent) were registered on a UV-Visible-1650 PC Shimadzu instrument, in transmission mode, in the 200-1100 nm wavelength range, at ambient temperature. The obtained data were used to calculate the energy gap values of nanoparticle solutions, according to Eq.(8) [20].

$$\text{Energy gap (eV)} = \frac{1240}{\lambda_{max}} \quad (8)$$

where, 1240 - the factor used to convert nm to eV;
λ_{max} - the maximum transmittance, nm.

The *infrared spectra* were registered on a FT-IR-8400S Shimadzu instrument, in transmission mode, in the 4000-400cm^{-1} range, at ambient temperature.

Wide-angle X-rays diffraction (WAXD) study was performed on a XRD-6000 Shimadzu instrument, with Bragg Brentano parafocusing goniometer. Scans were recorded in step mode using CuKα radiation (λ= 0.1541 nm). The working conditions were 40 kV and 30 mA tube power. The obtained diffraction data where mathematically treated to obtain structural information. The Scherrer equation (Eq.(9)) was used to calculate the size of the crystal particles.

$$D = K\lambda/\beta cos\,\theta \quad (9)$$

where, D - the size of crystalline;

k - the form factor (all most equal to 0.98);
λ - the wavelength of X-ray;
β - the full width at half maximum (FWHM) of an individual peak at 2Θ (where Θ is the Bragg angle) [21].

The lattice constants (a and c) of hexagonal system nanoparticles were estimated by using Eq.(10).

$$1/d_{hkl}^2 = \frac{4(h^2+hk+k^2)}{3a^2} + \left(l^2/c^2\right) \quad (10)$$

where, h, k, and l are Miller indices of a plane;
d_{hkl} is the interplanar spacing.

The lattice constant (a) values of cubic system nanoparticles were calculated according to Eq.(11).

$$1/d_{hkl}^2 = (h^2 + k^2 + l^2)/a^2 \quad (11)$$

Atomic force microscopy (AFM) was performed on an AFM-SPM-AA300 Shimadzu instrument, at ambient temperature.

Scanning electron (SEM) images were acquired with a TESCAN VEGA scanning electronic microscope, operating at a voltage of 30 kV with secondary and backscattering electrons in high vacuum mode.

Evaluation of adsorption of the nitrite ions onto the prepared nanoparticles

The nanoparticles of $Zn(OH)_2$ and $Ce(OH)_4$ (as-prepared), as well as ZnO and CeO_2 (annealed), were used to adsorb nitrite anions (NO_2^-) from aqueous solution and the absorbance at 362 nm was measured [22]. Three containers (50 mL) were marked T, B, and C respectively. Further, were added 5 mL of distilled water, 0.01 g of nanoparticles, and 0.6 mL of sodium nitrite solution ($1.55\cdot10^{-3}$ M). All samples were shaken and separated, then 1 mL of potassium iodide solution ($4.75\cdot10^{-5}$ M) with some drops of hydrochloric acid (37%), was added to all containers, as presented in Table 1. After 10 minutes, the absorbance at 362 nm was measured of each container, the reaction is explained according to Eq.(12).

$$2NaNO_2 + 2KI + 4HCl \rightarrow 2NO + 2NaCl + I_2 + 2KCl + 2H_2O \quad (12)$$

The percentage of nitrite pollution removal and efficiency can be calculated using Eqs.(13 and 14), respectively [17].

$$Removal\ rate(\%R) = [B - (C - T)/B] \times 100 \quad (13)$$

where, B stands for "blank", C for "control";
T for "test" as indicated in Table 1.

$$q_t = (B - T)\, v/w \quad (14)$$

where, v is the volume of nitrite solution (mL);
w is the weight of nanoparticles (g);
q_t is the adsorption capacity of prepared adsorbent in rapport with nitrite ions.

Results and discussion

Optical properties of the nanoparticles' solutions

The energy gap was determined using a plot of the optical transmission versus wavelength of nanoparticles for all samples (as-prepared and annealed), as illustrated in Figure 1.

Table 1

The weight and volumes require demonstrating the nitrite adsorption on the nanoparticles.

Reagent	*T*	*B*	*C*
nanoparticles (g)	0.01	-	0.01
distilled water (mL)	5	5	5
sodium nitrite (mL)	0.6	0.6	-
	Mix up with shaker for 15 min at 250 rpm then filtration		
potassium iodide (mL)	1	1	1
total volume (mL)	6.6	6.6	6.6

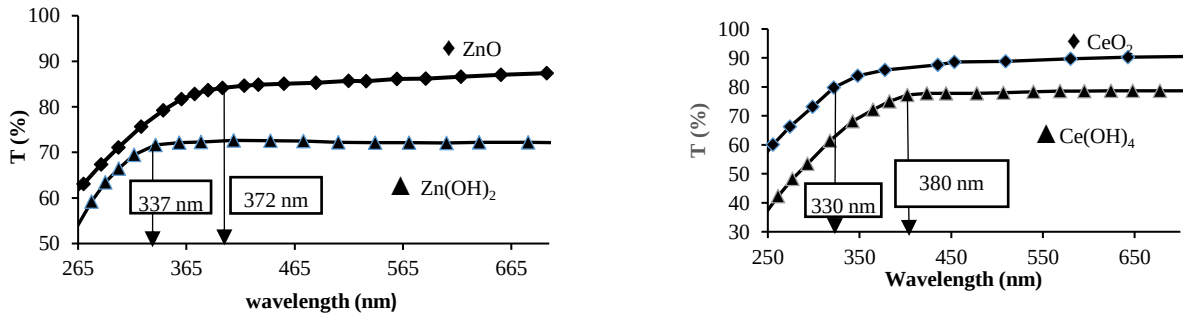

(a) *(b)*

Figure 1. The transmittance spectra for ZnO *(a)* and CeO_2 *(b)* nanoparticles solutions (obtained at the temperature range from 90°C to 400°C).

The permeability edge (redshift) of zinc hydroxide and zinc oxide nanoparticle solutions increases significantly from 337 nm (3.67 eV for $Zn(OH)_2$) to 372 nm (3.33 eV for ZnO), as shown in Figure 1*(a)*. These results are in concordance with the previously published work [23]. On the other hand, cerium hydroxide and cerium dioxide nanoparticles solutions, show an increase in transmittance edge to red shift from 330 nm (3.76 eV for $Ce(OH)_4$) to 380 nm (3.26 eV for CeO_2). These results are in concordance with the previously published paper [24], as shown in Figure 1(*b*).

Characterization of the nanoparticles by using FTIR method

The FTIR spectrum of the $Zn(OH)_2$ nanoparticles is presented in Figure 2*(a)*. The peak at 3310 cm^{-1} refers to O-H bond stretching vibration [25]. The peaks at 1047 cm^{-1} and 833 cm^{-1} relate to the stretching vibration of C-O and Zn-O, respectively [26]. The peaks at 468 cm^{-1} and 455 cm^{-1} correspond to Zn-O stretching and bending vibrations, respectively, of the $Zn(OH)_2$ nanoparticles [27,28]. The stretching peaks at 1502 cm^{-1} and 1390 cm^{-1} correspond to the stretching vibration of C=O, C-O, respectively [29]. Figure 2*(b)* shows the FTIR spectrum of ZnO. The broad bands at 3448 cm^{-1} and 1639 cm^{-1} are related to stretching and bending of the O-H bond in water, respectively. The peak at 570 cm^{-1} corresponds to the stretching of Zn-O [30].

The FTIR spectrum for $Ce(OH)_4$, Figure 2*(c)*, displays two bonds at 3473 cm^{-1} and 1644 cm^{-1} which are attributed to the stretching and bending vibrations of absorbed molecular water. The peak at 1506 cm^{-1} is due to the bending vibration of C=C for CTAB. The peak at 663 cm^{-1} corresponds to Ce-O stretching, while the peaks at 474-435 cm^{-1} correspond to the vibration of the O-Ce-O stretching. The FTIR of the CeO_2 nanoparticles is shown in Figure 2*(d)*. The peaks of about 3425 cm^{-1} and 1622 cm^{-1} are due to stretching and bending vibrations of absorbed molecules of water [31]. The peak at 1114 cm^{-1} corresponds to the vibration of the Ce-OH overtone band [32]. The tiny peak seen at 1055 cm^{-1} relates to the C-O component of the alcohol carried over to the sample. The broad peak between 560 cm^{-1} to 445 cm^{-1} is attributed to the O-Ce-O stretching vibration [33].

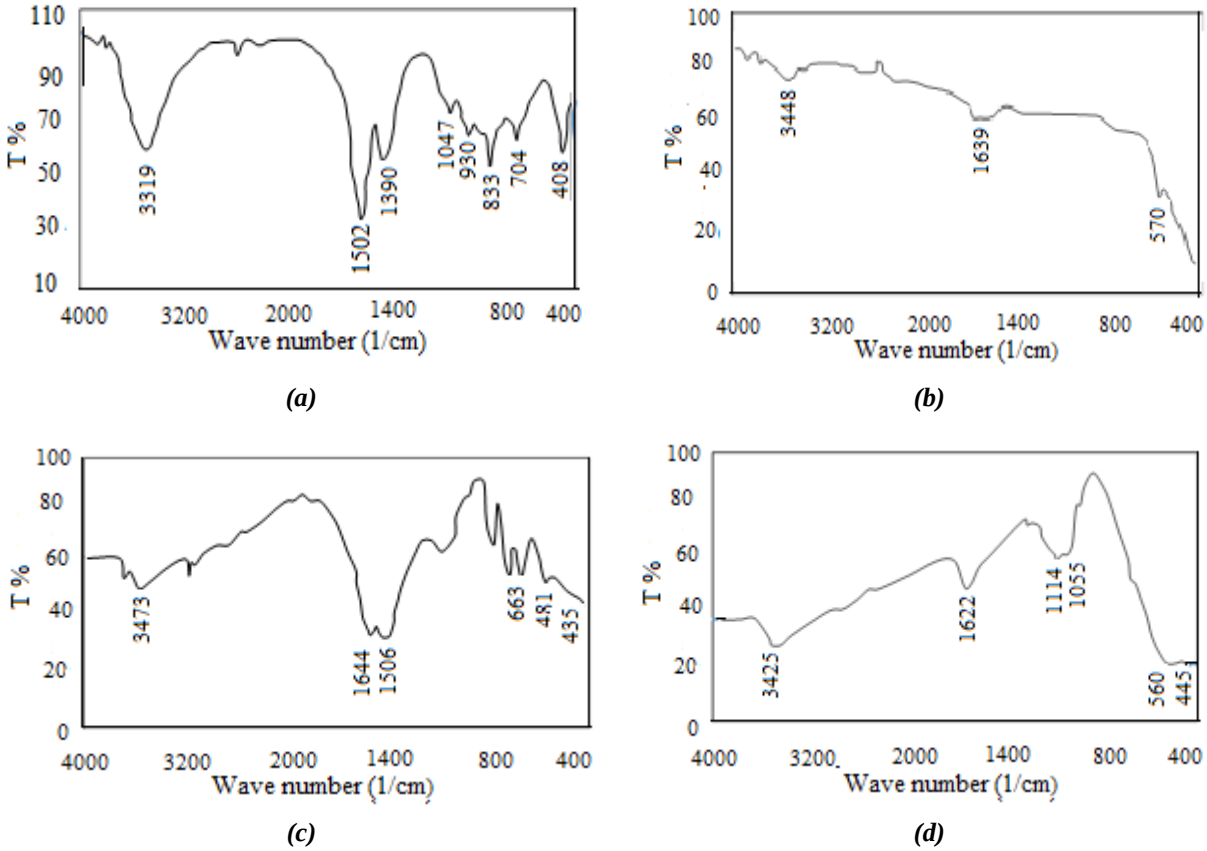

Figure 2. FTIR spectra for $Zn(OH)_2$ *(a)*, ZnO *(b)*, $Ce(OH)_4$ *(c)*, and CeO_2 *(d)* nanoparticles obtained at the temperature range from 90°C to 400°C.

XRD diffraction results

The X-ray diffraction pattern shows characteristic ZnO peaks at (*2θ*= 33.227°, 34.925°, 36.444°, 47.612°, 56.692°, 62.323°, and 67.980°), which correspond to the diffraction planes (100), (002), (101), (102), (110), (103), and (112), respectively, Figure 3. These peaks are indexed as the hexagonal wurtzite phase of ZnO nanoparticles with lattice constants *a*= *b*= 3.3046 Å and *c*= 5.0266 Å (JCPDS Card no.79–2205) and are compatible with that described in [34]. Furthermore, the XRD spectrum revealed no peaks other than the typical ZnO peaks. The $Zn(OH)_2$ peaks at (*2θ*= 33.227°, 34.925°, 36.444°, 47.612°, 56.692°, 62.323°,and 63.176°), which correspond to the diffraction planes (100), (002), (101), (102), (110), (103), and (112) respectively, this X-ray profile is very similar to ZnO results (JCPDS Card no. 01-089-0510) [35]. The size of the crystal particles and the lattice constants (*a* and *c*) of $Zn(OH)_2$ and ZnO nanoparticles are shown in Table 2.

The XRD results for $Ce(OH)_4$ are strikingly similar to those of CeO_2, with only a minor difference in intensity, indicating that CeO_2 is formed in both cases (Table 3). The main $Ce(OH)_4$ peaks at (*2θ*= 28.736°, 34.508°, 47.541°, 56.492°, 61.433°, and 69.341°), which correspond to the diffraction planes (111), (200), (220), (311), (222), and (400), could be attributed to the cubic shape, as indexed in (JCPDS Card no. 19-0284) [36].

Table 2

XRD results for $Zn(OH)_2$ and ZnO nanoparticles.

Nanoparticles	*2θ (°)*	*hkl*	*FWHM (°)*	*d (Å)*	*D (Å)*	*Lattice constants*	
						a (Å)	*c (Å)*
$Zn(OH)_2$	36.44	101	0.6381	2.4634	131.02	3.304	5.191
	33.05	100	0.6667	2.7077	124.25	-	-
	63.17	103	0.4071	1.4706	229.4	-	-
ZnO	36.33	101	0.6188	2.4706	135	3.243	5.206
	31.83	100	0.5437	2.8087	152.1		
	34.48	002	0.5542	2.5987	150		

Table 3

The XRD results for $Ce(OH)_4$ and CeO_2 nanoparticles.

Nanoparticles	*2θ (°)*	*hkl*	*FWHM (°)*	*d(Å)*	*D(Å)*	*Lattice constant, a (Å)*
$Ce(OH)_4$	28.730	111	0.43350	2.90713	189.9	5.413
	44.229	200	0.42700	2.04614	201.0	-
	47.501	220	0.64000	1.91256	135.5	-
CeO_2	28.6574	111	0.78310	3.11252	104.7	5.405
	47.5430	220	0.93460	1.91099	928.3	-
	56.4018	311	0.98100	1.63004	918.0	-

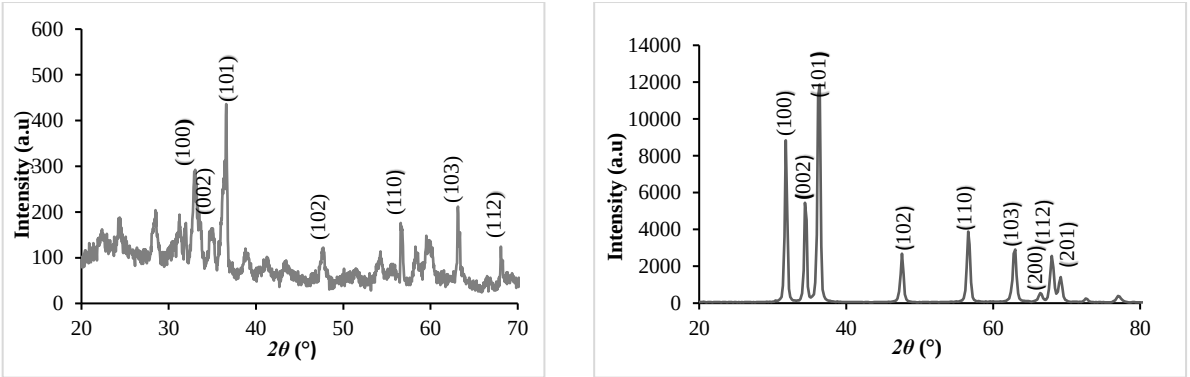

(a) JCPDS # 01-089-0510 ***(b) JCPDS # 79–2205***

Figure 3. XRD patterns of $Zn(OH)_2$ *(a)* and ZnO *(b)* nanoparticles obtained at the temperature range from 90°C to 400°C.

For CeO_2, the main peaks at (2θ= 28.657° , 34.150°, 47.543°, 56.401°, 61.512°, 69.548°, 75.619°, and 76.740°), which correspond to the diffraction planes (111), (200), (220), (311), (222), (400), (311), and (420), the same peaks emerged with increasing intensity of both, as indexed in (JCPDS Card No: 81–0792 [37]. The lattice constant values (a) for CeO_2 are presented in Figure 4 and Table 3.

Surface morphology of the obtained nanoparticles studied by atomic force microscopy

Figure 5 depicts AFM images of $Zn(OH)_2$ and ZnO nanoparticles, whose dispersion and accumulation change from an oval shape ($Zn(OH)_2$) Figure 5*(a)*, to the largest shape (ZnO), as shown in Figure 5*(b)*. This may be related to the conversion of most hydroxides to oxides during high-temperature heating (400°C).

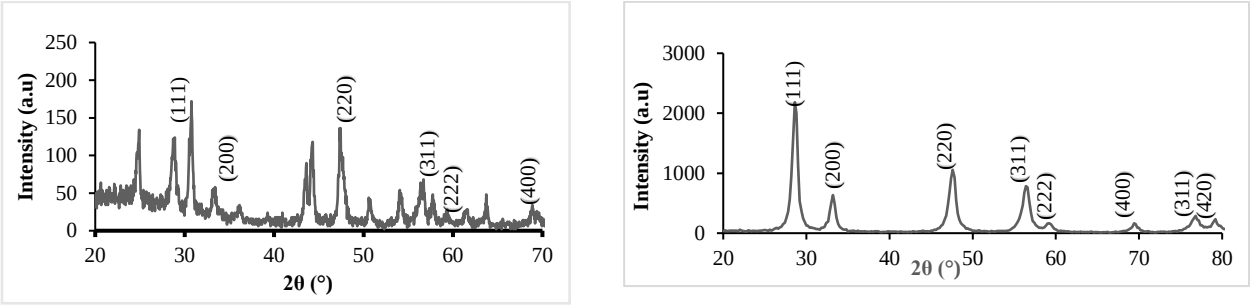

(a) *JCPDS # 19-0284* ***(b)*** *JCPDS # 81–0792*

Figure 4. XRD patterns of $Ce(OH)_4$ *(a)* and CeO_2 *(b)* nanoparticles obtained at the temperature range from 90°C to 400°C.

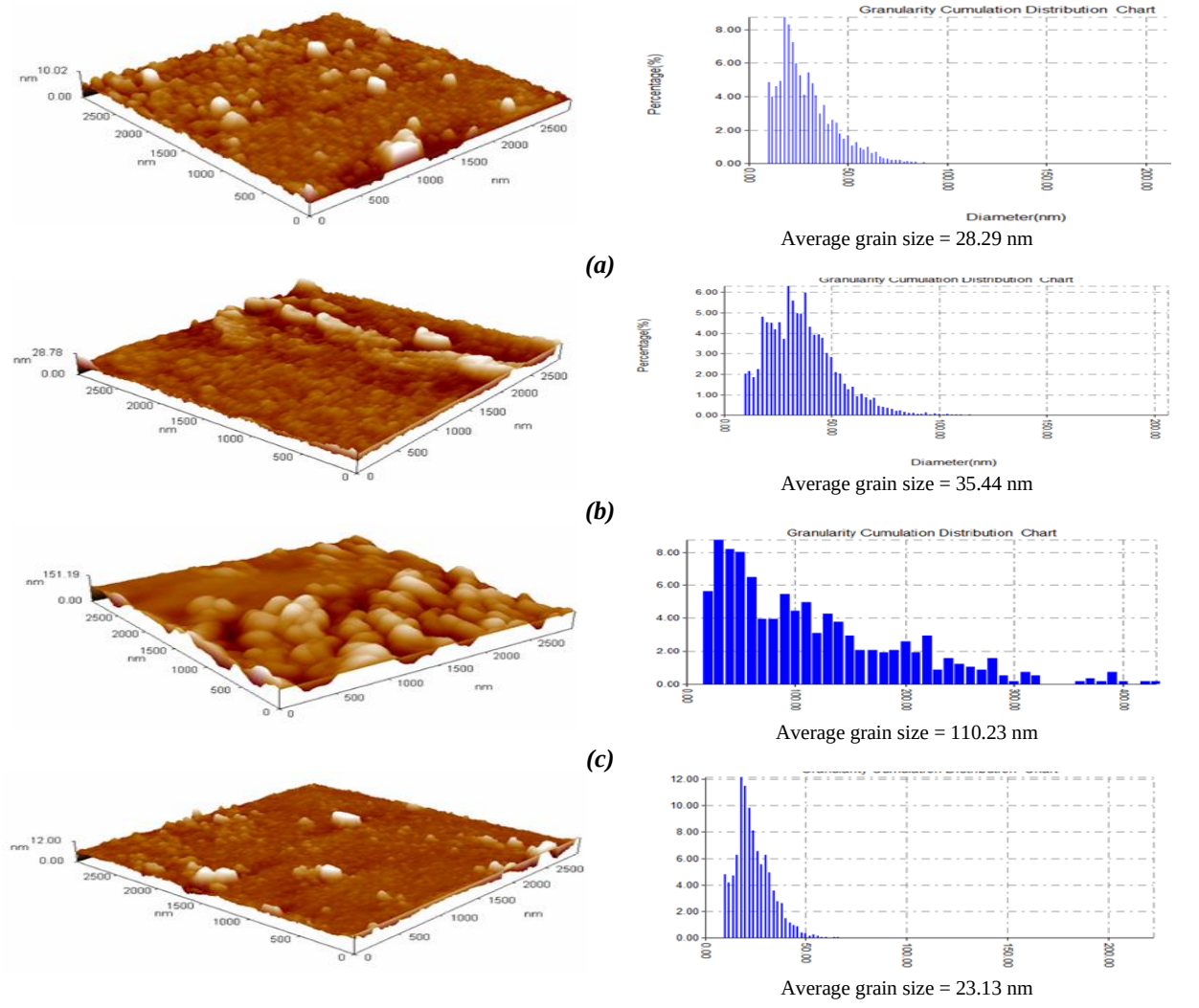

Figure 5. Three-dimensional atomic force microscopy images and granularity collection division charts of $Zn(OH)_2$ *(a)*, ZnO *(b)*, $Ce(OH)_4$ *(c)*, and CeO_2 *(d)* nanoparticles.

That is, during the preparation technique (autoclave), the product can be transformed into zinc oxide nanoparticles, and the grain size grows from 28.29 nm to 35.44 nm as the temperature rises.

Figure 5 shows AFM pictures of $Ce(OH)_4$ and CeO_2 nanoparticles which come in a variety of shapes that influence their distribution and accumulation. The $Ce(OH)_4$ sample resembles gigantic balls with an average grain size of 110.23 nm, Figure 5*(c)*, but after 400 °C annealing, the forms and grain size are reduced to 23.13 nm, Figure 5*(d)*, possibly due to the effect of temperature on the loss of water molecules from the sample and the conversion from the hydroxyl form to the oxide form, as described in Eq.(7).

Surface scanning electron microscopy investigations

The surface morphological investigation for ZnO and CeO_2 nanoparticles samples annealed at a temperature 400°C for 2 hours, was done using SEM analysis, and is shown in Figure 6. These analyses show a high porosity structure appearing on the sample's surfaces with an increase in the annealing temperature. Clusters of nanoparticles were seen on the surface, with a few aggregates. The SEM image of ZnO nanoparticles shows very wide particle size distribution and different morphologies of platelets and flaky particles, Figure 6*(a)*. On the other hand, the SEM images of CeO_2 nanoparticles appear to be nanoclusters, as presented in Figure 6*(b)*.

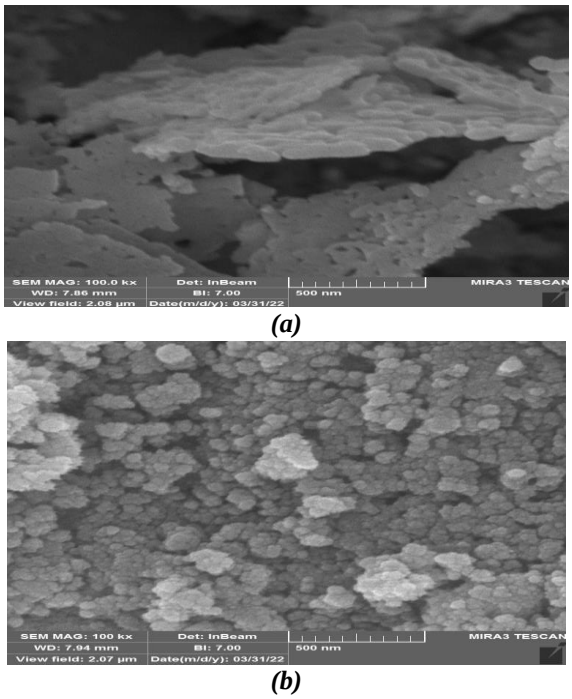

(a)

(b)

Figure 6. SEM images of annealing ZnO *(a)*, CeO_2 *(b)* nanoparticles annealed at 400°C for 2 hours.

Evaluation of possible applications of nanoparticles in the adsorption of nitrite ions

The results show that $Zn(OH)_2$ nanoparticles have the highest *%R* activity, while CeO_2 has the lowest one. The *%R* of nanoparticles was as follows: $Zn(OH)_2$> ZnO> $Ce(OH)_4$> CeO_2, as in Figure 7 and Table 4.

Table 4

Removal rate (*%R*) and the adsorption capacity (q_t) of the prepared nanoparticles

Nanoparticles	*Removal rate (%R)*		*Adsorption capacity (q_t)*	
	Hydroxide forms	*Oxide forms*	*Hydroxide forms*	*Oxide forms*
ZnO	59.50	37.09	155.52	89.61
CeO_2	32.75	33.58	54.03	79.67

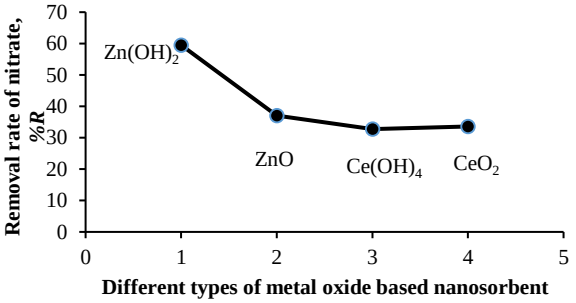

Figure 7. The removal rate (*%R*) of nitrites for different oxide based nanosorbents obtained in this study.

The significant decrease in *% R* for ZnO compared to $Zn(OH)_2$ from 59.50% to 37.09% is due to the higher activity of the hydroxide form ($Zn(OH)_2$) to nitrite removal than the annealed form (ZnO). The low adsorption of nitrite from aqueous solutions by $Ce(OH)_4$ from 32.75% to 33.58% for CeO_2 could be attributed to the higher average grain size for $Ce(OH)_4$ (110.23 nm) and lower surface area, thus causing decrease in *%R* activity. Whilst, the cerium dioxide nanoparticles have a lower average grain size (23.13 nm) and a higher surface area that cause increase in *%R* activity, as presented in Figure 5.

The q_t and *%R* of the nanoparticles have the same increasing sequences in comparison to the samples in hydroxide and oxide forms, as in Table 4. The highest adsorption capacity (q_t), was related to zinc oxide nanoparticles. With the exception of cerium hydroxide, we concluded that the *%R* and q_t of nitrite prefer to adsorb on hydroxide forms rather than on oxide forms, which may be related to the large differences in nanoparticle size between them.

This method differs from the previous methods, which depend on activated carbon modified by potassium permanganate and showed good adsorption ability for nitrate and nitrite ions from aqueous solutions [14], or during electrochemical oxidation of nitrite to nitrate by chlorine [37].

Conclusions

Different nanoparticles were prepared using the autoclave hydrothermal method. These nanoparticles were heated for one hour at 90°C to produce $Zn(OH)_2$ and $Ce(OH)_4$, and then annealed for two hours at 400°C to produce ZnO and CeO_2, respectively. The obtained nanoparticles where characterized by XRD, FTIR, UV–Visible, AFM, and SEM.

The results show that the average grain size of $Zn(OH)_2$ nanoparticles was 28.29 nm, which was smaller than that of ZnO nanoparticles, of 35.44 nm, and the ZnO morphology was platelet-like and flaky particles. Meanwhile, the average grain size of $Ce(OH)_4$ was 110.23 nm, much larger than that for CeO_2 nanoparticles, of 23.13 nm, and the morphology for CeO_2 nanoparticles appeared to be nanoclusters.

All hydroxide nanoparticles ($Zn(OH)_2$ and $Ce(OH)_4$) have higher $\%R$ and q_t for nitrite removal than oxide nanoparticles (ZnO and CeO_2). These results may be related to the adsorption of ions on the hydroxide surfaces of nanoparticles to form hydrogen bonding rather than on oxide surfaces.

Acknowledgements

The authors would like to express their appreciation to the Applied Science Department, University of Technology, Ministry of Higher Education and Scientific Research, Baghdad, Iraq for supporting this work.

References

1. Yedurkar, S; Maurya, C.; Mahanwar, P. Biosynthesis of zinc oxide nanoparticles using ixora coccinea leaf extract-A green approach. Open Journal of Synthesis Theory and Applications, 2016, 5(1), pp. 1-14. DOI: http://doi.org/10.4236/ojsta.2016.51001
2. Ranganatha, V.L.; Nithin, K.S.; Khanum, S.A.; Nagaraju, G.; Mallikarjunaswamy, C. Zinc oxide nanoparticles: A significant review on synthetic strategies, characterization and applications. AIP Conference Proceedings, 2019, 2162(1), pp. 0200089-6. DOI: http://doi.org/ 10.1063/1.5130299
3. Aldalbahi, A.; Alterary, S.; Almoghim, R.A.A; Awad, M.A.; Aldosari, N.S.; Alghannam, S.F.; Alabdan, A.N.; Alharbi, S.; Alateeq, B.A.M.; Al Mohsen, A.A.; Alkathiri, M.A.; Alrashed, R.A. Greener synthesis of zinc oxide nanoparticles: characterization and multifaceted applications. Molecules, 2020, 25(18), pp. 1–14. DOI: http://doi.org/10.3390/molecules25184198
4. Halbos, R.J.; Al-Algawi, S.; Rasheed, R.T. Synthesis and characterization of IZO composite prepared by sol-gel method. Journal of Al-Nahrain University, 2016, 19(3), pp. 39–47. DOI: http://doi.org/10.22401/JNUS.19.3.06
5. Alwan, R.M.; Kadhim, Q.A.; Sahan, K.M.; Ali, R.A.; Mahdi, R.J.; Kassim, N.A.; Jassim, A.N. Synthesis of zinc oxide nanoparticles via Sol – Gel route and their characterization. Nanoscience and Nanotechnology, 2015, 5(1), pp. 1–6. DOI: http://doi.org/10.5923/j.nn.20150501.01
6. Lira-Cantu, M.; Norrman, K.; Anderasen, J.W.; Krebs, F.C. Oxygen release and exchange in niobium oxide MEHPPV hybrid solar cells. Chemistry of Materials, 2006, 18(24), pp. 5684–5690. DOI: http://doi.org/10.1021/cm061429d
7. Niu, J.; Azfer, A.; Rogers, L.M.; Wang, X.; Kolattukudy, P.E. Cardioprotective effects of cerium oxide nanoparticles in a transgenic murine model of cardiomyopathy. Cardiovascular Research, 2007, 73(3), pp. 549–559. DOI: https://doi.org/10.1016/j.cardiores.2006.11.031
8. Abdullah, T.A.; Juzsakova, T.; Rasheed, R.T.; Mallah, M.A.; Salman, A.D.; Cuong, Le P.; Jakab, M.; Zsirka, B.; Kułacz, K.; Sebestyén, V. V_2O_5, CeO_2 and their MWCNTs nanocomposites modified for the removal of Kerosene from water. Nanomaterials, 2022, 12(2), pp. 189–209. DOI: https://doi.org/10.3390/nano12020189
9. Alabyadh, T.; Albadri, R.; Es-haghi, A.; Yazdi, M.E.T.; Ajalli, N.; Rahdar, A.; Thakur, V.K. ZnO/CeO_2 nanocomposites: metal-organic framework-mediated synthesis, characterization, and estimation of cellular toxicity toward liver cancer cells. Journal of Functional Biomaterials, 2022, 13(3), pp. 139–151. DOI: https://doi.org/10.3390/jfb13030139
10. Farhangi, M.J.; Es-haghi, A.; Yazdi, M.E.T.; Rahdar, A.; Baino, B. MOF-mediated synthesis of CuO/CeO_2 composite nanoparticles: characterization and estimation of the cellular toxicity against breast cancer cell line (MCF-7). Journal of Functional Biomaterials, 2021, 12(4), pp. 53–65. DOI: https://doi.org/10.3390/jfb12040053
11. Ghorani-Azam, A.; Mottaghipisheh, J.; Amiri, MS.; Mashreghi, M.; Hashemzadeh, A.; Haddad-Mashadrizeh, A.; Nourbakhsh, F.; Nadaf, M.; Qayoomian, M.; Yazdi, M.E.T.; Vitalini, S.; Iriti, M. Resveratrol-mediated gold-nanoceria synthesis as green nanomedicine for phytotherapy of hepatocellular carcinoma. Frontiers in Bioscience-Landmark, 2022, 27(8), pp. 227-233. DOI: https://doi.org/10.31083/j.fbl2708227
12. Hanafi, A.H.; Azeema, S.M.A. Removal of nitrate and nitrite anions from wastewater using activated

carbon derived from rice straw. Journal of Environmental & Analytical Toxicology, 2016, 6(1), pp. 1–6. DOI: https://doi.org/10.4172/2161-0525.1000346
13. Gauthama, B.U; Narayana, B.; Sarojini, B.K.; Bello, K.; Suresh, N.K. Nitrate/Nitrite determination in water and soil samples accompanied by in situ azo dye formation and its removal by superabsorbent cellulose hydrogel.
14. Zatar, N.A.; Abu-Eid, M.A.; Eid, A.F. Spectrophotometric determination of nitrite and nitrate using phosphomolybdenum blue complex. Talanta, 1999, 50(4), pp. 819–826. DOI: http://doi.org/10.1016/s0039-9140(99)00152-6
15. Wang, Q.-H.; Yu, L.-J.; Liu, Y.; Lin, L.; Lu, R.-G.; Zhu, J.-P.; He, L.; Lu, Z.-L. Methods for the detection and determination of nitrite and nitrate: A review. Talanta, 2017, 165, pp. 709–720. DOI: http://doi.org/10.1016/j.talanta.2016.12.044
16. Suneetha, M.; Ravindhranath, K. Adsorption of nitrite ions from wastewater using bio-sorbents derived from Azadirachta indica Plant. Asian Journal of Water, Environmental and Pollution. 2017, 14(2), pp. 71–79. DOI: http://doi.org/10.3233/AJW-170017
17. Suzaimi, N.D.; Goh, P.S.; Malek, N.A.N.N.; Lim, J.W.; Ismail, A.F. Performance of branched polyethyleneimine grafted porous rice husk silica in treating nitrate-rich wastewater *via* adsorption. Journal of Environmental Chemical Engineering, 2019, 7(4), pp. 103235. DOI: http://doi.org/10.1016/j.jece.2019.103235
18. Altowayti, W.A.H.; Allozy, H.G.A.; Shahir, S.; Goh, P.S.; Yunus, M.A.M. A novel nanocomposite of aminated silica nanotube (MWCNT/Si/NH_2) and its potential on adsorption of nitrite. Environmental Science Pollution Research, 2019, 26(28), pp. 28737–28748. DOI: http://doi.org/10.1007/s11356-019-06059-0
19. Majeed, A.A.; Rasheed, R.T. Preparation, characterization and nanozymes activity of ZnO and SnO2 nanoparticles. Natural Volatiles and Essential Oils, 2021, 8(4), pp. 12805–12822. https://nveo.org/index.php/journal/article/view/2702
20. Abdul-Zahra, Z.J.; Rasheed, R.T. Preparation, characterization, and ninhydrin removal by Al_2O_3 and V_2O_5 nanoparticles. Journal of Medicinal and Chemical Sciences, 2023, 6(2), pp. 376–391. DOI: https://doi.org/10.26655/JMCHEMSCI .2023.2.18
21. Thipwimonmas, Y.; Jaidam, J.; Samoson, K.; Khunseeraksa, V.; Phonchai, A.; Thiangchanya, A.; Chang, K.H.; Abdullah, A.F.L.; Limbut, W. A simple and rapid spectrophotometric method for nitrite detection in small sample volumes. Chemosensors, 2021, 9(7), pp. 161–168. DOI: http://doi.org/10.3390/chemosensors9070161
22. Rini, A.S.; Rati, Y.; Maisita, S.W. Of ZnO nanoparticle using sandoricum koetjape peel extract as bio-stabilizer under microwave irradiation. Journal of Physics: Conference Series, 2021, 2049(1), pp. 7–14. DOI: http://doi.org/10.1088/1742-6596/2049/1/012069
23. Mahabadi, A.G.; Mirzakhani, A.; Azizi, A.; Chavoshi, S.; Khaghani, Sh. Extracts of Pelargonium hortorum: A natural and efficient fluid for fast and eco-friendly biosynthesis of CeO_2 nanoparticles for antioxidant and photocatalytic applications. Inorganic Chemistry Communications, 2021, 127, pp. 108553. DOI: http://doi.org/10.1016/j.inoche.2021.108553
24. Zafar, M.N.; Dar, Q.; Nawaz, F.; Zafar, M.N.; Iqbal, M.; Nazar, M.F. Effective adsorptive removal of azo dyes over spherical ZnO nanoparticles. Journal of Materials Research and Technology, 2019, 8(1), pp. 713–725. DOI: http://doi.org/10.1016/j.jmrt.2018.06.002
25. Jan, H.; Shah, M.; Usman, H.; Khan, M.; Zia, M.; Hano, C.; Abbasi, B.H. Biogenic synthesis and characterization of antimicrobial and antiparasitic zinc oxide (ZnO) nanoparticles using aqueous extracts of the Himalayan Columbine (*Aquilegia pubiflora*). Frontiers in Materials, 2020, 7, pp. 1–14. DOI: http://doi.org/10.3389/fmats.2020.00249
26. Singh, S.C. Effect of oxygen injection on the size and compositional evolution of ZnO/$Zn(OH)_2$ nanocomposite synthesized by pulsed laser ablation in distilled water. Journal of Nanoparticle Research, 2011, 13(9), pp. 4143–4152. DOI: http://doi.org/10.1007/s11051-011-0359-2
27. Handore, K.; Bhavsar, S.; Horne, A.; Chhattise, P.; Mohite, K.; Ambekar, J.; Pande, N.; Chabukswar, V. Novel green route of synthesis of ZnO nanoparticles by using natural biodegradable polymer and its application as a catalyst for oxidation of aldehydes. Journal Macromolecular Science, Part A, 2014, 51(12), pp. 941–947. DOI: http://doi.org/10.1080/10601325.2014.967078
28. Jayarambabu, N.; Kumari, B.S.; Rao, K.V.; Prabhu, Y.T. Germination and growth characteristics of mungbean seeds (*Vigna radiata* L) affected by synthesized zinc oxide nanoparticles. International Journal of Current Engineering and Technology, 2014, 4(5), pp. 3411–3416. http://inpressco.com/wp-content/uploads/2014/09/Paper593411-3416.pdf
29. Umar, A.; Kumar, R.; Kumar, G.; Algarni, H.; Kim, S.H. Effect of annealing temperature on the properties and photocatalytic efficiencies of ZnO nanoparticles. Journal of Alloys and Compounds, 2015, 648, pp. 46–52. DOI: http://doi.org/10.1016/j.jallcom.2015.04.236
30. Prabaharan, D.M.D.M.; Sadaiyandi, K.; Mahendran, M.; Sagadevan, S. Structural, optical, morphological and dielectric properties of cerium oxide nanoparticles. Materials Research, 2016, 19(2), pp. 478–482. DOI: http://dx.doi.org/10.1590/1980-5373-mr-2015-0698
31. Kannan, S.K; Sundrarajan, M. A green approach for the synthesis of a cerium oxide nanoparticle: characterization and antibacterial activity.

International Journal of Nanoscience, 2014, 13(03), pp. 1450018.
DOI: http://doi.org/10.1142/s0219581x14500185

32. Pujar, M.S; Hunagund, S.M; Desai, V.R; Patil, S; Sidarai, A.H. One-step synthesis and characterizations of cerium oxide nanoparticles in an ambient temperature via Co-precipitation method. AIP Conference Proceedings, 2018, 1942(1), pp. 50026–4.
DOI: http://doi.org/10.1063/1.5028657
33. Baghdadi, A.M.; Saddiq, A.A.; Aissa, A.; Algamal, Y.; Khalil, N.M. Structural refinement and antimicrobial activity of aluminum oxide nanoparticles. Journal of Ceramic Society of Japan, 2022, 130(3), pp. 257–263.
DOI: http://doi.org/10.2109/jcersj2.21140
34. Kashinath, L.; Namratha, K.; Byrappa, K. Microwave assisted facile hydrothermal synthesis and characterization of zinc oxide flower grown on graphene oxide sheets for enhanced photodegradation of dyes. Applied Surface Science, 2015, 357, Part B, pp. 1849–1856.
DOI: http://doi.org/10.1016/j.apsusc.2015.09.072
35. Bindu, P.; Thomas, S. Estimation of lattice strain in ZnO nanoparticles: X-ray peak profile analysis. Journal of Theoretical and Applied Physics, 2014, 8(4), pp. 123–134.
DOI: http://doi.org/10.1007/s40094-014-0141-9
36. Tumkur, P.P.; Gunasekaran, N.K; Lamani, B.R; Bayon, N.N.; Prabhakaran, K.; Hall, J. C.; Ramesh, G. T. Cerium oxide nanoparticles: synthesis and characterization for biosafe applications. Nanomanufacturing, 2021, 1(3), pp. 176–189. DOI: http://doi.org/10.3390/nanomanufacturing1030013
37. Tamizhdurai, P.; Sakthinathan, S.; Chen, S.-M.; Shanthi, K.; Sivasanker, S.; Sangeetha, P. Environmentally friendly synthesis of CeO_2 nanoparticles for the catalytic oxidation of benzyl alcohol to benzaldehyde and selective detection of nitrite. Scientific Reports, 2017, 7(1), pp. 1–13.
DOI: http://doi.org/10.1038/srep46372